LOSS MECHANISMS IN SIW AND MSIW

N. Ranjkesh and M. Shahabadi

Faculty of Electrical and Computer Engineering
University of Tehran
Tehran, Iran

Abstract—In this paper, the power dissipated through different loss mechanisms including dielectric, conductor and radiation loss is calculated for the substrate integrated waveguide (SIW) and modified substrate integrated waveguide (MSIW). The applied computational method being appropriate for structures with periodic conducting parts allows one to calculate the integrals corresponding to these powers analytically and with high accuracy.

1. INTRODUCTION

The substrate integrated waveguide (SIW) is a promising waveguide structure which maintains the advantages of the rectangular waveguide (RW), such as high Q-factor and high power handling capability in planar form [1–7]. In the SIW, two periodic rows of plated via-holes are embedded in the substrate. They along with the top and bottom metallic layers of the substrate introduce a structure similar to the common RWs (Fig. 1).

Evidently, the propagation characteristics of the SIW cannot be determined successfully without considering the effects of the power dissipated in its dielectric and radiated through periodic gaps between the adjacent vias. They reduce its Q-factor in comparison to a hollow RW [8].

Since in the SIW, the inner part of the waveguide is filled with a dielectric material, it can be predicted that dielectric loss plays an important role in the total dissipation power. For reduction of dielectric losses in the SIW, a new structure called modified substrate integrated waveguide (MSIW) was introduced in which some part of the dielectric of the substrate between periodic sidewalls has been removed (Fig. 1) [9]. The manufacturing process of this waveguide is also introduced in [9]. The present work concerns with an exact
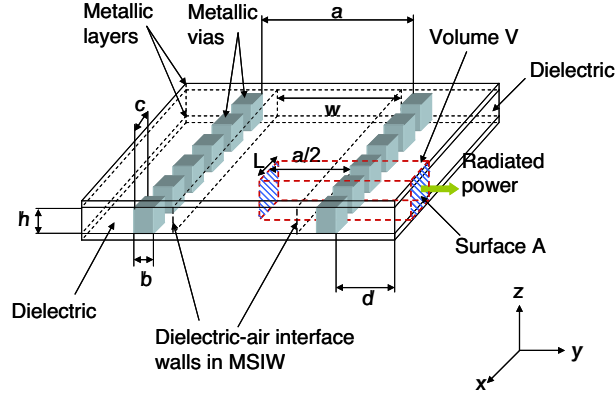
Figure 1. Substrate integrated waveguide. Volume V and surface A, used in power calculations, are shown in this figure.

quantitative analysis of the SIW and MSIW in order to specify the main cause of losses at a given frequency.

2. METHOD OF ANALYSIS

The method introduced in [9, 10] is adopted for this work. In this method, dividing the structure into a number of homogeneous dielectric and periodic conductor-dielectric regions and expressing the electromagnetic fields in each region as a summation of proper basis functions, whose coefficients satisfy the transmission line (TL) equations, the full-wave analysis of the periodic structure is reduced to the circuit analysis of the equivalent cascaded TL model.

2.1. Dispersion Diagrams

According to the Floquet theorem, the pseudo-Fourier nature of the electromagnetic fields in a periodic structure allows us to express the total fields as pseudo-Fourier series expansions. In our structure which is periodic in the x direction, this property leads to the following series expansions:

$$\vec{E}\left(\vec{r}\right) = \lim_{M \to \infty} \sum_{m=-M}^{M} \vec{E}_m\left(y,\,z\right) e^{-\left(j\frac{2m\pi}{L}+k_x\right)x} \tag{1}$$

$$\vec{H}\left(\vec{r}\right) = \lim_{M \to \infty} \sum_{m=-M}^{M} \vec{H}_m\left(y,\,z\right) e^{-\left(j\frac{2m\pi}{L}+k_x\right)x} \tag{2}$$

in which $k_x = j\beta + \alpha$ denotes the complex propagation constant of the waveguide mode and L is the period of the structure (Fig. 1).

Since in the SIW, the height of the substrate (h) is very small in comparison to the distance between periodic metallic walls (a), there are no changes with respect to z for the modes with the lowest cut-off frequencies. So we can reduce our analysis to a two-dimensional one. In the two-dimensional analysis with variations in the x and y directions, there are two groups of modes: TE_x with E_z, H_x, and H_y components, and TM_x with H_z, E_x, and E_y components. Between these two groups of modes, only TE_x ones satisfy the necessary boundary conditions on the surfaces of the top and bottom metallic layers of the substrate. In other words, we begin our analysis with the two-dimensional TE_x modes with no variations with respect to z and satisfy the entire necessary boundary conditions on the surfaces of the vias; since in this analysis, there is no tangential electric field component in the x-y plane, all necessary boundary conditions on the surfaces of the top and bottom metallic layers are automatically satisfied and because of no variations with respect to z, these modes have the lowest cut-off frequencies.

These modes are denoted by TE_{0n} modes, in which n is the number of changes in the y direction between the two periodic walls and 0 represents the number of changes in the z direction. Maxwell's equations for TE_{0n} are reduced to three scalar equations as follow:

$$\frac{\partial E_z}{\partial y} = -j\omega\mu_0 H_x \tag{3}$$

$$\frac{\partial E_z}{\partial x} = -j\omega\mu_0 H_y \tag{4}$$

$$\frac{\partial H_y}{\partial x} - \frac{\partial H_x}{\partial y} = j\omega(\varepsilon' - j\varepsilon'')E_z \tag{5}$$

By reducing our analysis to the two-dimensional case, we have to study the structure in Fig. 2. As shown in this picture, we divide our structure into homogeneous dielectric and periodic conductor-dielectric layers in the y direction. Note that we have assumed rectangular via-holes for the sake of simplicity; however, via-holes of circular cross-section can equally be treated if one approximates curved walls with fine rectilinear boundaries.

As mentioned earlier, in each layer we express the total electromagnetic fields as a summation of proper basis functions. For homogeneous layers, we use the space harmonics expressed in Equations (1) and (2), as basis functions. By substitution of these expansions in Maxwell's equations for a homogeneous layer of ($\varepsilon' - j\varepsilon''$, μ), we obtain a system of first order differential equations for the
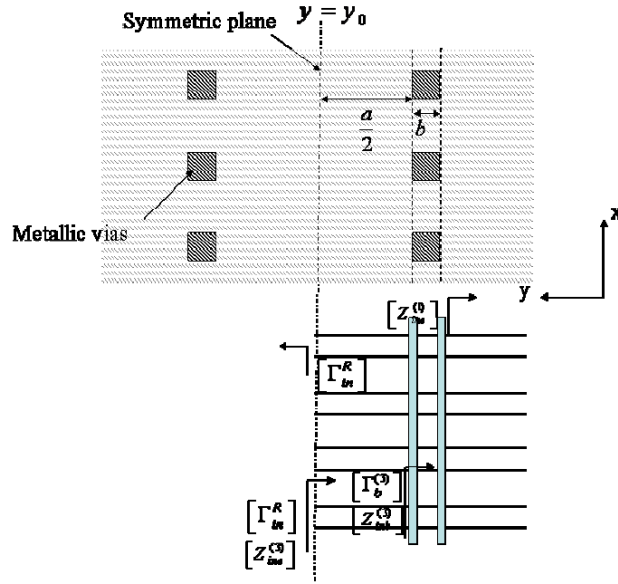
Figure 2. Two dimensional view of SIW and its equivalent network model.

coefficients of each space harmonic. For the m-th space harmonic, these equations are expressed as:

$$\frac{\partial}{\partial y} E_{zm}(y) = -j\omega\, L_m H_{xm}(y) \tag{6}$$

$$\frac{\partial}{\partial y} H_{xm}(y) = -(j\omega C_m + G_m) E_{zm}(y) \tag{7}$$

in which:

$$L_m = \mu \tag{8}$$

$$C_m = \varepsilon_0 \left(\alpha^2 - \left(\frac{2m\pi}{L} + \beta \right)^2 \right) / k_0^2 + \varepsilon' \tag{9}$$

$$G_m = -2\omega\varepsilon_0\alpha \left(\beta + \frac{2m\pi}{L} \right) / k_0^2 + \omega\varepsilon'' \tag{10}$$

These equations show that a homogeneous layer with $(\varepsilon' - j\varepsilon'',\, \mu)$ can be substituted by a system of infinite number of TLs each with capacitance, conductance, and inductance C_m, G_m, and L_m, respectively. Voltages and currents of the TLs represent the coefficients

of the m-th space harmonic of E_z and H_x, respectively. For all the homogeneous layers, we use the same formulation.

For periodic conductor-dielectric layers, the total fields in dielectric regions can be expressed as a summation of local modes $\tilde{\phi}_n$. By assuming that the width of the gaps between two adjacent vias is d and that the gap is centred at $x = x_0$, the functions $\tilde{\phi}_n$ are expressed as:

$$\tilde{\phi}_n = \cos(n\pi(x - x_0)/d) \tag{11}$$

For the n-th local mode the following equations express the relations between the coefficients:

$$\frac{d}{dy}\tilde{E}_{zn}(y) = -j\omega\tilde{L}_n\tilde{H}_{xn}(y) \tag{12}$$

$$\frac{d}{dy}\tilde{H}_{xn}(y) = -\left(j\omega\tilde{C}_n + \tilde{G}_n\right)\tilde{E}_{zn}(y) \tag{13}$$

in which $\tilde{E}_{zn}$, $\tilde{H}_{xn}$, and $\tilde{H}_{yn}$ are the coefficients of the corresponding electromagnetic field components, and the coefficients $\tilde{C}_n$, $\tilde{G}_n$, and $\tilde{L}_n$ are defined as:

$$\tilde{L}_n = \mu \tag{14}$$

$$\tilde{C}_n = -\varepsilon_0\left(\frac{n\pi}{d}\right)^2/k_0^2 + \varepsilon' \tag{15}$$

$$\tilde{G}_n = \omega\varepsilon'' \tag{16}$$

Obviously, for this layer of the structure, there is also an equivalent model of infinite number of TLs with parameters $\tilde{C}_n$, $\tilde{G}_n$, and $\tilde{L}_n$.

Finally to establish the continuity condition of the electromagnetic fields on the interface between two adjacent layers with different basis functions, we use the mode matching technique by expanding one set of basis functions in terms of the others and vice versa [11–13], while for adjacent layers with similar basis functions, these conditions are reduced to the continuity conditions of the voltages and currents of the equivalent cascaded TLs.

Using the mode matching technique, the continuity condition for E_z and H_x components reduces to the matrix relations between the coefficients of the basis functions or equivalently between the voltages and currents of the equivalent TLs. Finally, the complete equivalent network is composed of a cascaded circuit of TLs in which the successive layers with different basis functions are connected by the multi-port networks (Fig. 2). For interfaces with similar basis functions these equivalent TLs are directly connected.

Since in practice the number of equivalent TLs for each layer is limited, these numbers are chosen in a proper manner to satisfy the necessary condition for applying mode matching technique in the interfaces between layers with different basis functions [11]. For our structure, this condition is expressed as $\frac{2M}{L} \approx \frac{N}{d}$, in which N is the number of local modes in the periodic region and M is expressed according to Equations (1) and (2).

The solutions of $V_m(y)$ and $I_m(y)$ for each equivalent TL are known, but because of the effect of the multi-port networks, the variables $V_m(y)$ and $I_m(y)$ for the m-th TL in a specific layer are related to the variables $V_{m'}(y)$ and $I_{m'}(y)$ for the m'-th TL in that particular layer. The continuity conditions for the voltages and currents of the equivalent network help us to determine all the unknown vectors $[V^+(y)]$ and $[V^-(y)]$, namely the forward and backward voltages for each equivalent TL. If we consider the plane $y = y_0$ as the reference plane, the following equation holds.

$$\left[V^-(y_0)\right] = \left[\Gamma_{in}^R\right]\left[V^+(y_0)\right] \tag{17}$$

In this equation, matrix $[\Gamma_{in}^R]$ is the reflection matrix evaluated from the right TLs and has all the necessary information looking to the right. Similar relation is true if we look to the left from this reference plane:

$$\left[V^+(y_0)\right] = \left[\Gamma_{in}^L\right]\left[V^-(y_0)\right] \tag{18}$$

where the matrix $[\Gamma_{in}^L]$ is calculated looking to the left TLs from this reference plane. The Equations (17) and (18) have nonzero solutions if the following condition is satisfied [14]:

$$\det\left(\left[\Gamma_{in}^R\right]\left[\Gamma_{in}^L\right] - I\right) = 0 \tag{19}$$

This equation is only a function of variables α, β, and ω and can be used to extract dispersion properties of the waveguide.

2.2. Calculation of Dissipating Powers

To calculate dialectic losses, the value $\frac{1}{2}\omega\varepsilon''|E|^2$ is integrated within the volume occupied by the dielectric parts, while conductor losses are evaluated using the integration of $\frac{1}{2}R_s|H_s|^2$ on the surfaces of the metallic vias as well as the top and bottom metallic surfaces. In these terms, ω, ε'', R_s, $|E|$ and $|H_s|$ are, respectively, the frequency (rad/m), the imaginary part of the dielectric permittivity, the surface resistance of the metal and magnitudes of the electric and the tangential magnetic

fields. According to Floquet's theorem and because of the symmetry of the structure, evaluating these integrals can be limited to the one symmetrical half of a period. Radiation losses are evaluated integrating the term $\frac{1}{2}\vec{E} \times \vec{H}^*$ on the surface A in Fig. 1. Dielectric and conductor losses are evaluated within the volume V in Fig. 1. By obtaining the expansion coefficients appearing in the equivalent circuit model, the corresponding integrals in each region can be expressed as an algebraic summation of the analytical solutions. In evaluation of some of these integrals Perseval's formula can help to simplify the calculation.

3. RESULTS

The attenuation constants of the SIW and MSIW structures considered on RO4003C ($\varepsilon_r = 3.38$, $\tan(\delta) = 0.0027$) and RT5880 ($\varepsilon_r = 2.2$, $\tan(\delta) = 0.0009$) substrates are shown in Fig. 2. For RO4003C substrate $a = 8$ mm, $L = 2$ mm and $w/a = 0.9$ and for RT5880 substrate $a = 10$ mm, $L = 2.2$ mm and $w/a = 0.9$. Other parameters are selected as $b = c = 0.8$ mm and $h = 31$ mil for all structures. All metallic parts are considered as copper with $\sigma = 5.6 \times 10^7$ S/m. The via-holes have rectangular cross sections for simplicity. As is obvious in these diagrams, the attenuation constants of the MSIW structures on both substrates are almost flat by changing frequency and have significant reduction in respect to the conventional SIWs on the same substrates. For the SIW on RT5880 substrate the results obtained by HFSS and calibration [15] are also shown in Fig. 2 for comparison.

   Figure 3 shows the normalized powers lost through different mechanisms, including dielectric losses (P_D), conductor losses (P_C), and radiation losses (P_R) of the SIW and MSIW structures on RO4003C substrate. These powers are normalized with respect to the total dissipated power so that $P_D + P_C + P_R$ is unity. As it is obvious from these diagrams, dielectric losses are the most important factor of power dissipation in the SIW (about 70–85 percent of the total dissipated power) and the portion of this factor increases by increasing frequency. After this factor, conductor losses form about the 18–28 percent of the total dissipated power, whereas radiation losses are the less important dissipation factor which can be disregarded consequently. For the MSIW, the losses in decreasing order of significance are conductor losses, radiation losses, and dielectric losses. The reduction of dielectric losses below radiation losses is significant in this waveguide. The amount of power dissipated in dielectric increases by increasing frequency which is obvious because of the linear relation between dielectric losses and $\omega\varepsilon''$. As a result, the flat slope of the attenuation constant of the MSIW can be explained accordingly due
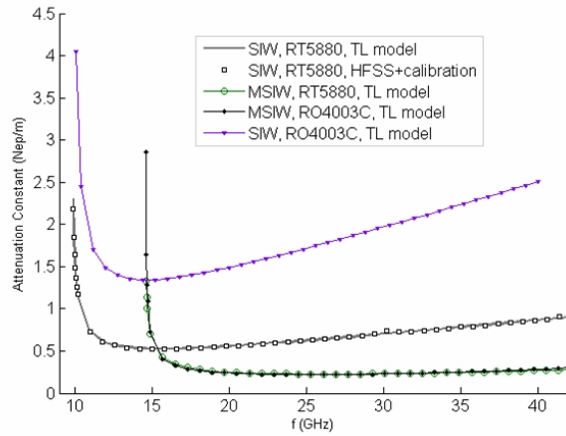
Figure 3. Attenuation constants of the SIW and MSIW structures on two common substrates.
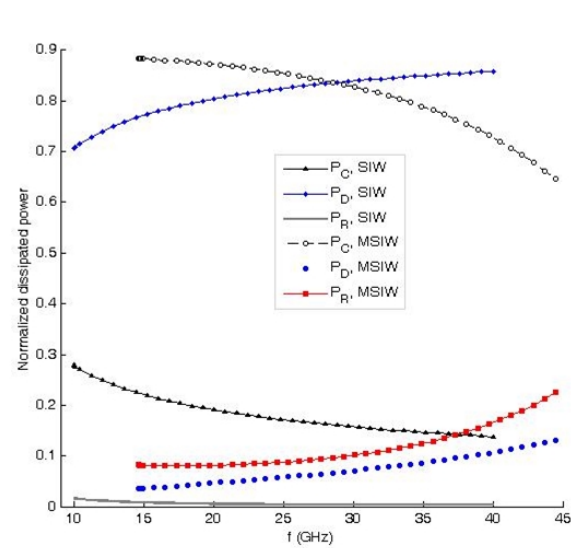

Figure 4. Normalized dissipated powers for the SIW and MSIW structures on RO4003C substrate.

to the reduced impact of dielectric losses on the MSIW.

Figure 4 shows the same diagrams for RT5880 substrate. For this dielectric, similar results are obtained and dielectric losses still are the most important dissipation factor in a wide range of frequencies.

However, they are less significant in comparison to RO4003C substrate. Also, in this case embedding an air-cut in the structure causes a significant reduction of dielectric losses. In all these calculations $d = 20$ mm.

It is also an important point to mention that different factors can change the portions corresponding to different mechanisms. Since in SIW and MSIW $h \ll a$, there are no changes with respect to z for the modes with the lowest cutoff frequencies. When calculating attenuated powers caused by different loss mechanisms, dielectric and radiation losses as well as the portion of conductor losses related to the surfaces of vias are all proportional to h, while conductor losses of the top and bottom metallic layers are independent of h. As a result, the contribution of conductor losses increases by reducing h. In the cases mentioned above, reducing the height of the substrate to a lower value of $h = 20$ mil, for the SIW on RT5880 substrate increases the contribution of conductor losses such that the intersection of the two diagrams corresponding to P_D and P_C shifts from 12 GHz at $h = 31$ mil case to 23 GHz at $h = 20$ mil. However, for the SIW on RO4003C substrate, h has no significant effect, and dielectric losses are still the most significant dissipation mechanism. As expected, the fraction of power dissipated by radiation increases by increasing the period of the waveguide, but as long as its value remains in the typical range, its effect is not very significant.
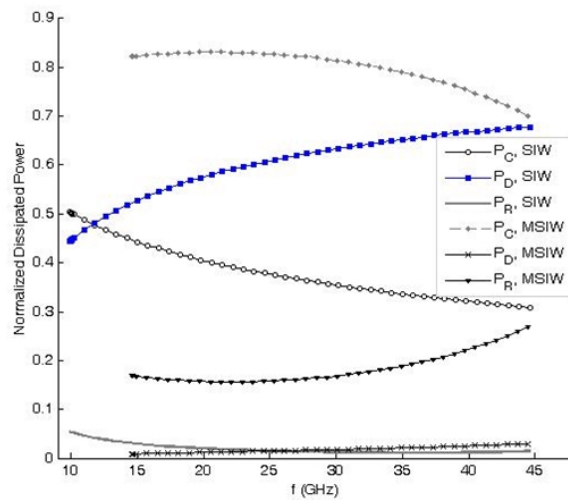

Figure 5. Normalized dissipated powers for the SIW and MSIW structures on RT5880 substrate.

4. CONCLUSION

As mentioned in this letter, in the SIW, dielectric loss usually is the most important factor of power dissipation; however, by introducing an air-cut in the SIW in the form of the MSIW, its influence can be reduced significantly. In MSIW, which offers a higher Q-factor, the major power dissipation is due to conductor loss.

REFERENCES

1. Hirokawa, J. and M. Ando, "Single-layer feed waveguide consisting of posts for plane TEM wave excitation in parallel plates," *IEEE Trans. Antennas Propagat.*, Vol. 46, No. 5, 625–630, May 1998.

2. Cassivi, Y. and K. Wu, "Substrate integrated circuits concept applied to the nonradiative dielectric guide," *IEE Proc. Microw. Antennas Propag.*, Vol. 152, No. 1, 424–433, Feb. 2005.

3. Han, S., X.-L. Wang, Y. Fan, Z. Yang, and Z. He, "The generalized chebyshev substrate integrated waveguide diplexer," *Progress In Electromagnetics Research*, PIER 73, 29–38, 2007.

4. Zhang, X.-C., Z.-Y. Yu, and J. Xu, "Novel band-pass substrate integrated waveguide (SIW) filter based on complementary split ring resonators (CSRRs)," *Progress In Electromagnetics Research*, PIER 72, 39–46, 2007.

5. Talebi, N. and M. Shahabadi, "Application of generalized multipole technique to the analysis of discontinuties in substrate integrated waveguides," *Progress In Electromagnetics Research*, PIER 69, 227–235, 2007.

6. Deslandes, D., Y. Cassivi, K. Wu, L. Perregrini, P. Arcioni, M. Bressan, and G. Conciauro, "Field analysis and design model of substrate integrated waveguide," *2002 Progress in Electromagn. Res. Symp. Proc.*, Singapore, Jan. 7–10, 2002.

7. Wu, K., "Design models and circuit interconnects of substrate integrated rectangular waveguide (SIRW) components," *2002 Progress in Electromagn. Res. Symp. Proc.*, Singapore, Jan. 7–10, 2002.

8. Desland, D. and K. Wu, "Integrated transition of coplanar to rectangular waveguides," *IEEE MTT-S Int. Microwave Simp. Dig.*, Vol. 2, 619–622, Feb. 2001.

9. Ranjkesh, N. and M. Shahabadi, "Reduction of dielectric losses in substrate integrated waveguide," *IEE Electronics Letters*, Vol. 42, 1230–1231, Oct. 2006.

10. Ghazi, G. and M. Shahabadi, "Modal analysis of extraordinary transmission through an array of subwavelength slits," *Progress In Electromagnetics Research*, PIER 79, 59–74, 2008.

11. Mittra, R. and S. W. Lee, *Analytical Techniques in the Theory of Guided Waves*, 30–50, Macmillan, New York, 1971.

12. Eleftheriades, G. V., A. S. Omar, and L. P. B. Katehi, "Some important properties of waveguide junction generalized scattering matrices in the context of the mode matching technique," *IEEE Trans. Microwave Theory Tech.*, Vol. 42, No. 10, 1896–1903, Oct. 1994.

13. Collmann, R. R. and F. M. Landstorfer, "Calculation of the field radiated by horn-antennas using the mode-matching method," *IEEE Trans. Antennas Propagat.*, Vol. 43, No. 8, 876–880, Aug. 1995.

14. Kashani, Z. G., N. Hojjat, and M. Shahabadi, "Full-wave analysis of coupled waveguides in a two-dimensional photonic crystal," *Progress In Electromagnetics Research*, PIER 49, 291–307, 2004.

15. Xu, F. and K. Wu, "Guided-wave and leakage characteristics of substrate integrated waveguide," *IEEE Trans. Microwave Theory Tech.*, Vol. 53, No. 1, 66–73, Jan. 2005.